X-641-70-426
PREPRINT

COMPUTER STUDY OF CONVECTION OF WEAKLY IONIZED PLASMA IN A NONUNIFORM MAGNETIC FIELD

JENG-NAN SHIAU

DECEMBER 1970

GODDARD SPACE FLIGHT CENTER
GREENBELT, MARYLAND

Computer Study of Convection of Weakly Ionized Plasma in a Nonuniform Magnetic Field

Jeng-Nan Shiau*

Research Associate
Laboratory for Space Physics
Goddard Space Flight Center
Greenbelt, Maryland

*Presently a National Academy of Sciences-National Research Council Research Associat pursuing associateship at Goddard Space Flight Center.

ABSTRACT

A weakly ionized plasma in a strong and nonuniform magnetic field exhibits an instability analogous to the flute instability in a fully ionized plasma. The instability sets in at a critical magnetic field. To study the final state of the plasma after the onset of the instability, we numerically integrate the plasma equations assuming a certain initial spectrum of small disturbances. In the regime we studied, numerical results indicate a final steadily oscillating state consisting of a single finite amplitude mode together with a time independent modification of the original equilibrium. Our numerical results agree with the analytic results obtained by Simon in the slightly super-critical regime. As the magnetic field is increased further, the wavelength of the final oscillation becomes nonunique. There exists a subinterval in the unstable wave band. Final stable oscillation with a wavelength in this subinterval can be established if the initial disturbance has a sufficiently strong component at the particular wavelength.

1. Introduction

The information one obtains from a linear stability analysis is the critical value of some external parameter for the onset of the instability and the wavelengths of the modes which begin to grow. After a period of exponential growth of the unstable modes to finite amplitudes, the linearized equation with the assumption of infinitesimal perturbation is no longer valid.

To learn the ultimate fate of the excited modes and the final state of the plasma, a nonlinear treatment is necessary. In the case of instabilities in a weakly ionized plasma obeying simple moment equations, Simon[1] has developed a general theory describing the final oscillating state of the plasma. The initially stable plasma is assumed to become unstable upon small fractional increase Δ of some external parameter. By expanding with respect to the small parameter Δ, the final amplitudes of the steadily oscillating states, the frequency shifts and the time independent change in the equilibrium distribution can be determined in terms of Δ.

Another possible approach to the nonlinear stability problem is through numerical integration of the plasma equations using a computer. One assumes a certain initial spectrum of small disturbances and studies its development in time to learn the behavior of the plasma upon onset of instability. The work of Sato and Tsuda[2] is such a study of the cross-field instability.

In this paper, using a similar computational approach, we study the nonlinear evolution of an instability which causes the convective flow of a weakly ionized plasma in a strong and nonuniform magnetic field. Part of this problem has been discussed by Kadomtsev[3] in the quasi-linear approximation. Nonlinear analytic results describing the final steadily oscillating states in the slightly super-critical regime, $\Delta \ll 1$, have also been obtained by

Simon[4] using the general theory of Ref. 1. However, the computational approach has the advantage of not involving the assumption of small super-criticality. Thus we can study the behavior of the plasma as the external parameter is increased further from its critical value for the onset of the instability. This is the purpose of the present investigation in addition to comparing the numerical results in the slightly super-critical regime with the analytic results of Ref. 4 (hereafter referred to as I).

The instability we studied is analogous to the flute instability in a fully ionized plasma. Consider a weakly ionized plasma filling the space between two infinitely long concentric cylinders (cf. Fig. 1). Let us assume that an azimuthal magnetic field $\underset{\sim}{H}$, decreasing along the radius as $1/r$, exists in the space between the cylinders and that in the equilibrium state all quantities vary in the radial direction only. The oppositely directed drifts of electrons and ions in the nonuniform field produce no charge separation in the equilibrium state. However, a z-dependent density perturbation will produce charge separation and associated electric fields. The resultant $\underset{\sim}{E} \times \underset{\sim}{H}$ drifts, coupled with an appropriate equilibrium radial density gradient, can cause growth of the initial perturbations. Diffusion due to collisions with the background neutrals tends to smooth out these perturbations and hence the magnetic field has to exceed a certain critical value for the instability to occur.

In Sec. 2, we write down the basic equations of the system and describe the equilibrium state as given in I. We then write the equations governing the perturbations and give a brief account of the linear stability analysis. The perturbation equations are properly scaled in Sec. 3. We then expand the perturbations in Fourier series and arrive at an initial value problem involving an infinite number of interacting modes. In carrying out the

numerical integration on an IBM 360 computer, we approximate the system by one with a finite number of modes and consider initial white-noise-like or weighted small perturbations. The time development of these perturbations at various magnetic field strengths above the critical field is presented in Sec. 4 and Sec. 5. We give a final discussion in Sec. 6. In the regime we studied, our computed results indicate a final steadily oscillating state with the dominance of a single finite amplitude mode together with a time independent modification of the equilibrium distribution. The final oscillating state approaches that given in I when the magnetic field is slightly above its critical value.

2. Basic Equations and Linear Stability Analysis

We consider a weakly ionized plasma filling the space between two conducting grounded long cylinders with radii R and R + d respectively, where $d \ll R$ (cf. Fig. 1). We will assume quasineutrality, i.e. the number densities of electrons and ions are equal. Ionization at the two cylinders is achieved in such a way that a constant density s is maintained at the inner cylinder and a density $s - \delta s$ at the outer cylinder, where $\delta s \ll s$. There is also an applied strong steady toroidal magnetic field produced by a current flowing along the inner cylinder. If we assume the plasma current to be negligible, by Maxwell's equations the magnetic field $\underset{\sim}{H}$ is in the θ direction with intensity decreasing as $1/r$.

Since the density of the charged particles is considerably lower than the density of neutral particles, we can assume that the neutral component is stationary. We shall describe the behavior of electrons and ions by the equation of continuity and the equation of motion of each species. They have the form

$$\frac{\partial n}{\partial t} + \nabla\cdot(n\underset{\sim}{v}^{\pm}) = 0 \tag{2.1}$$

$$T^{\pm}\nabla n = \mp en\nabla\varphi \pm \frac{en}{c}(\underset{\sim}{v}^{\pm}\times\underset{\sim}{H}) - \frac{nm^{\pm}\underset{\sim}{v}^{\pm}}{\tau^{\pm}} \tag{2.2}$$

where the superscripts + and - refer to ions and electrons respectively. Here n is the species number density, $\underset{\sim}{v}$ the average velocity, T the temperature, e the absolute value of electron charge, φ the electric field potential, m the mass, and τ is the average collision time with the background gas. The upper sign choice in these equations is for ions, the lower is for electrons. In writing these equations we have assumed that the plasma is quasineutral ($n^{+} \approx n^{-} = n$) and the temperature of each species is maintained spatially uniform by frequent collisions with the background neutral gas. We also assumed that the frequencies of the motion we study are much less than the collision frequencies so that the inertia term can be ignored. The electric field is presumed electrostatic in nature.

We can solve for $n\underset{\sim}{v}^{\pm}$ from Eq. (2.2) and substitute the results into Eq. (2.1). We obtain two equations for the determination of n and φ. In cylindrical coordinates these equations have the form

$$\begin{aligned}
&\frac{\partial n}{\partial t} + \frac{1}{r}\frac{\partial}{\partial r}\left[r\left(-D_{\perp}^{\pm}\frac{\partial n}{\partial r} \mp nb_{\perp}^{\pm}\frac{\partial\varphi}{\partial r}\right)\right] \\
&+ \frac{1}{r}\frac{\partial}{\partial\theta}\left(-D^{\pm}\frac{1}{r}\frac{\partial n}{\partial\theta} \mp nb^{\pm}\frac{1}{r}\frac{\partial\varphi}{\partial\theta}\right) + \frac{\partial}{\partial z}\left(-D_{\perp}^{\pm}\frac{\partial n}{\partial z} \mp nb_{\perp}^{\pm}\frac{\partial\varphi}{\partial z}\right) \\
&\pm (\Omega^{\pm}\tau^{\pm})\left[\frac{\partial}{\partial z}\left(-D_{\perp}^{\pm}\frac{\partial n}{\partial r} \mp nb_{\perp}^{\pm}\frac{\partial\varphi}{\partial r}\right) - \frac{\partial}{\partial r}\left(-D_{\perp}^{\pm}\frac{\partial n}{\partial z} \mp nb_{\perp}^{\pm}\frac{\partial\varphi}{\partial z}\right)\right] = C
\end{aligned} \tag{2.3}$$

where $\nabla \times \underset{\sim}{H} = 0$ has been assumed. Here for each species $b = e\tau/m$ is the mobility, $D = T\tau/m$ the diffusion coefficient, and $b_\perp$ and $D_\perp$ represent b and D each divided by $1 + (\Omega\tau)^2$ where $\Omega = eH/mc$ is the cyclotron frequency. The magnetic field is assumed to be so strong that $(\Omega\tau)^2 \gg 1$ for both electrons and ions.

We shall repeat here the definition of the equilibrium state as given in I. Let us consider an equilibrium in which the density and the potential are functions of r only. Eq. (2.3) reduces to

$$\frac{1}{r}\frac{d}{dr}\left[r\left(-D_\perp^{\pm}\frac{dN}{dr} \mp N b_\perp^{\pm}\frac{dV}{dr}\right)\right] = 0$$

where N and V are the equilibrium density and potential respectively. Making use of the fact $D_\perp \sim H^{-2} \sim r^2$ as is $b_\perp$ and eliminating the $b_\perp$ terms between the two equations implied above, one finds that

$$\frac{1}{r^3}\frac{d}{dr}\left(r^3\frac{dN}{dr}\right) = 0$$

and hence

$$N = A + B\, r^{-2}$$

The corresponding equation for V is

$$\frac{dV}{dr} = \frac{\text{const.}}{r^3 N}$$

Since N is positive in the region of integration and since V must vanish at both ends, we must have

$$V \equiv 0 \qquad (2.4)$$

Adjusting the constants on N to fit the boundary conditions, one has

$$N = s - \frac{\delta s\,(R+d)^2}{(R+d)^2 - R^2}\left[1 - \left(\frac{R}{r}\right)^2\right] \tag{2.5}$$

It can be shown that a necessary condition for the instability is that Nr^2 decrease in the outward direction. Hence, to assure that we have such a configuration, we require that

$$s \ll \frac{\delta s\,(R+d)^2}{(R+d)^2 - R^2}$$

or expanding

$$\frac{\delta s}{s} \gg \frac{2d}{R} \tag{2.6}$$

Henceforth, we can use the approximation

$$\frac{1}{r^2}\frac{d}{dr}(r^2 N) \cong -\frac{\delta s}{d} \tag{2.7}$$

Let us now consider a density perturbation n_1 (r, z, t) and a potential perturbation V_1(r, z, t) superimposed on the above equilibrium state. No θ dependence of the perturbation quantities is assumed since we expect the most unstable mode to be of the interchange type with no variation along the magnetic field. Substituting

$$n = N(r) + n_1\,(r, z, t)$$

$$\varphi = V(r) + V_1\,(r, z, t)$$

into Eq. (2.3) and making use of the properties of the equilibrium solution, we arrive at the following equations governing the perturbations.

$$\frac{\partial n_1}{\partial t} - \frac{1}{r}\frac{\partial}{\partial r}(rD_\perp^\pm \frac{\partial n_1}{\partial r}) - \frac{\partial}{\partial z}(D_\perp^\pm \frac{\partial n_1}{\partial z})$$

$$\pm(\Omega^\pm\tau^\pm)\frac{\partial}{\partial r}(D_\perp^\pm \frac{\partial n_1}{\partial z}) \mp (\Omega^\pm\tau^\pm)\frac{\partial}{\partial z}(D_\perp^\pm \frac{\partial n_1}{\partial r})$$

$$\mp \frac{1}{r}\frac{\partial}{\partial r}\left[r(N+n_1)b_\perp^\pm \frac{\partial V_1}{\partial r}\right] \mp \frac{\partial}{\partial z}\left[(N+n_1)b_\perp^\pm \frac{\partial V_1}{\partial z}\right]$$

$$+ (\Omega^\pm\tau^\pm)\left\{\frac{\partial}{\partial r}\left[(N+n_1)b_\perp^\pm \frac{\partial V_1}{\partial z}\right] - \frac{\partial}{\partial z}\left[(N+n_1)b_\perp^\pm \frac{\partial V_1}{\partial r}\right]\right\} = 0$$

Since $D_\perp \sim H^{-2} \sim r^2$ as is $b_\perp$, we may write

$$\frac{\partial n_1}{\partial t} - D_\perp^\pm\left[\frac{1}{r^3}\frac{\partial}{\partial r}(r^3\frac{\partial n_1}{\partial r}) + \frac{\partial^2 n_1}{\partial z^2}\right] \pm (\Omega^\pm\tau^\pm)D_\perp^\pm \frac{\partial n_1}{\partial z}$$

$$\mp b_\perp^\pm\left[\frac{1}{r^3}\frac{\partial}{\partial r}(r^3 N\frac{\partial V_1}{\partial r}) + N\frac{\partial^2 V_1}{\partial z^2}\right] + (\Omega^\pm\tau^\pm)b_\perp^\pm \frac{1}{r^2}\frac{\partial}{\partial r}(r^2 N)\frac{\partial V_1}{\partial z}$$

$$\mp b_\perp^\pm\left[\frac{1}{r^3}\frac{\partial}{\partial r}(r^3 n_1\frac{\partial V_1}{\partial r}) + \frac{\partial}{\partial z}(n_1\frac{\partial V_1}{\partial z})\right]$$

$$+ (\Omega^\pm\tau^\pm)b_\perp^\pm\left[\frac{1}{r^2}\frac{\partial}{\partial r}(r^2 n_1\frac{\partial V_1}{\partial z}) - \frac{\partial}{\partial z}(n_1\frac{\partial V_1}{\partial r})\right] = 0 \qquad (2.8)$$

By virtue of the boundary conditions, we expect $\partial n_1/\partial r$ to be of order n_1/d and similarly $\partial V_1/\partial r$ to be of order V_1/d. In Eqs. (2.8) r-derivatives may therefore be brought through r-dependent coefficients and allowed to act directly on $\partial n_1/\partial r$, $\partial V_1/\partial r$, $n_1(\partial V_1/\partial r)$ and $n_1(\partial V_1/\partial z)$. The neglected terms (involving r-derivatives of the coefficients) are small compared to those retained in the parameter d/R or $\delta s/s$. Hence using Eq. (2.7) one obtains

$$\frac{\partial n_1}{\partial t} - D_\perp^\pm(\frac{\partial^2 n_1}{\partial r^2} + \frac{\partial^2 n_1}{\partial z^2}) \pm \frac{T^\pm}{e}\frac{c}{H}\frac{2}{r}\frac{\partial n_1}{\partial z} \mp b_\perp^\pm N(\frac{\partial^2 V_1}{\partial r^2} + \frac{\partial^2 V_1}{\partial z^2})$$

$$- \frac{c}{H}\frac{\delta s}{d}\frac{\partial V_1}{\partial z} \mp b_\perp^\pm\left[\frac{\partial}{\partial r}(n_1\frac{\partial V_1}{\partial r}) + \frac{\partial}{\partial z}(n_1\frac{\partial V_1}{\partial z})\right]$$

$$+ \frac{c}{H}\left[\frac{\partial}{\partial r}(n_1\frac{\partial V_1}{\partial z}) - \frac{\partial}{\partial z}(n_1\frac{\partial V_1}{\partial r})\right] = 0$$

The coefficient of each term is a very weak function of r in the annular region and may be assumed constant. Defining $x = r - R$ and neglecting small quantities of order d/R, we may write

$$\frac{\partial n_1}{\partial t} - D_\perp^{\pm}\left(\frac{\partial^2 n_1}{\partial x^2} + \frac{\partial^2 n_1}{\partial z^2}\right) \pm \frac{T^{\pm}}{e}\frac{c}{H}\frac{2}{h}\frac{\partial n_1}{\partial z} \mp b_\perp^{\pm} s\left(\frac{\partial^2 V_1}{\partial x^2} + \frac{\partial^2 V_1}{\partial z^2}\right)$$
$$- \frac{c}{H}\frac{\delta s}{d}\frac{\partial V_1}{\partial z} \mp b_\perp^{\pm}\left[\frac{\partial}{\partial x}\left(n_1\frac{\partial V_1}{\partial x}\right) + \frac{\partial}{\partial z}\left(n_1\frac{\partial V_1}{\partial z}\right)\right]$$
$$+ \frac{c}{H}\left[\frac{\partial}{\partial x}\left(n_1\frac{\partial V_1}{\partial z}\right) - \frac{\partial}{\partial z}\left(n_1\frac{\partial V_1}{\partial x}\right)\right] = 0 \qquad (2.9)$$

Eqs. (2.9) are the approximate equations governing the perturbation quantities n_1 and V_1.

Let us now consider infinitesimal perturbations, when terms involving products of n_1 and V_1 become negligible. The resulting linearized equations and the boundary conditions suggest perturbations of the form $\sin(n\pi x/d)\exp(i\omega t + ikz)$ where n is any positive integer and k is the axial wave number. Substituting perturbations of the above form into the linearized version of Eqs. (2.9) and solving for the real and imaginary parts of ω, we find[4]

$$\omega^R = \frac{kc}{H}\left[\frac{2}{eR}(T^- b_\perp^+ - T^+ b_\perp^-) + \frac{\delta s}{sd}(D_\perp^- - D_\perp^+)\right](b_\perp^+ + b_\perp^-)^{-1}$$

$$\omega^I = \frac{(k^2+\kappa^2)^2 (D_\perp^+ b_\perp^- + D_\perp^- b_\perp^+) - (2\delta s/sdeR)(kc/H)^2(T^+ + T^-)}{(k^2+\kappa^2)(b_\perp^+ + b_\perp^-)} \qquad (2.10)$$

where $\kappa = n\pi/d$. The imaginary part of ω is negative at large value of H and the instability can occur. The neutrally stable state occurs when

$$(\Omega^+ T^+)(\Omega^- T^-) = \frac{(k^2+\kappa^2)^2}{k^2\kappa^2}\frac{(n\pi)^2}{2}\frac{R}{d}\frac{s}{\delta s} \qquad (2.11)$$

The right-hand side is a minimum for $k = \kappa = \pi/d$. Hence the critical field H_c at which the instability sets in is given by

$$(\Omega^+\tau^+)(\Omega^-\tau^-) = 2\pi^2 \frac{R}{d}\frac{s}{\delta s}$$

which is much larger than unity, in accord with our initial assumptions. Solving for H_c, we find

$$H_c^2 = \frac{2\pi^2 c^2}{b^+ b^-}\frac{R}{d}\frac{s}{\delta s} \tag{2.12}$$

In Fig. 2, we plot on the H-k plane the neutral stability curves representing $\omega^I = 0$ for various values of n. The plasma is linearly stable for $H < H_c$. Modes with small wavenumber do not produce sufficient polarization electric field for their growth while modes with too large a wavenumber are damped out by diffusion. So the instability first sets in only with the critical wavenumber $k_c = \pi/d$ and $n = 1$ at $H = H_c$.

3. Machine Calculation

In this paper, we are concerned with the development of finite amplitude motion for $H > H_c$. We shall integrate the full Eqs. (2.9) in time on a computer, assuming small initial perturbations, and look into the ultimate fate of these perturbations.

The perturbation equations will first be put into dimensionless form. We take the characteristic length in the x and z directions to be d and Λd respectively, where Λ is an adjustable parameter. The characteristic time is taken to be the approximate period t* of the critical mode in the limit of $b^+ \ll b^-$ and $T^+ \approx T^-$,

$$t^* = \frac{2d^2}{T^+}\frac{eH}{c}\frac{s}{\delta s} \tag{3.1}$$

Making use of the following dimensionless variables,

$$\begin{aligned} \eta &= x/d \\ \xi &= z/(\Lambda d) \\ \tau &= t/t^* \\ \rho &= n_1/\delta s \\ \Psi &= V_1/\left(\frac{T^+}{e}\frac{\delta s}{s}\right) \end{aligned} \tag{3.2}$$

We obtain from Eqs. (2.9),

$$\begin{aligned} \frac{\partial \rho}{\partial \tau} = {} & A_1\left(\frac{\partial^2 \rho}{\partial \eta^2} + \frac{1}{\Lambda^2}\frac{\partial^2 \rho}{\partial \xi^2}\right) - A_2\frac{1}{\Lambda}\frac{\partial \rho}{\partial \xi} \\ & + A_1\left(\frac{\partial^2 \Psi}{\partial \eta^2} + \frac{1}{\Lambda^2}\frac{\partial^2 \Psi}{\partial \xi^2}\right) + \frac{2}{\Lambda}\frac{\partial \Psi}{\partial \xi} \\ & + A_3\left[\frac{\partial}{\partial \eta}\left(\rho\frac{\partial \Psi}{\partial \eta}\right) + \frac{1}{\Lambda^2}\frac{\partial}{\partial \xi}\left(\rho\frac{\partial \Psi}{\partial \xi}\right)\right] \\ & - \frac{2}{\Lambda}\left[\frac{\partial}{\partial \eta}\left(\rho\frac{\partial \Psi}{\partial \xi}\right) - \frac{\partial}{\partial \xi}\left(\rho\frac{\partial \Psi}{\partial \eta}\right)\right] \end{aligned} \tag{3.3}$$

$$\begin{aligned} & B_1\left(\frac{\partial^2 \rho}{\partial \eta^2} + \frac{1}{\Lambda^2}\frac{\partial^2 \rho}{\partial \xi^2}\right) - B_2\frac{1}{\Lambda}\frac{\partial \rho}{\partial \xi} \\ & + B_3\left(\frac{\partial^2 \Psi}{\partial \eta^2} + \frac{1}{\Lambda^2}\frac{\partial^2 \Psi}{\partial \xi^2}\right) \\ & + B_4\left[\frac{\partial}{\partial \eta}\left(\rho\frac{\partial \Psi}{\partial \eta}\right) + \frac{1}{\Lambda^2}\frac{\partial}{\partial \xi}\left(\rho\frac{\partial \Psi}{\partial \xi}\right)\right] = 0 \end{aligned} \tag{3.4}$$

where

$$\begin{aligned} A_1 &= 2\,b_\perp^+\frac{H}{c}\frac{s}{\delta s} \\ A_2 &= \frac{4d}{R}\frac{s}{\delta s} \\ A_3 &= \frac{2H}{c}b_\perp^+ \end{aligned} \tag{3.5}$$

$$B_1 = \frac{2H}{c}\frac{s}{\delta s}\left(b_\perp^+ - b_\perp^- \frac{T^-}{T^+} \right)$$

$$B_2 = \frac{4d}{R}\frac{s}{\delta s}\left(1 + \frac{T^-}{T^+} \right)$$

$$B_3 = \frac{2H}{c}\frac{s}{\delta s}\left(b_\perp^+ + b_\perp^- \right)$$

$$B_4 = \frac{2H}{c}\left(b_\perp^+ + b_\perp^- \right)$$

Eq. (3.3) is obtained from the ion version of Eqs. (2.9) and Eq. (3.4) is obtained by eliminating $\partial n_1/\partial t$ between the two Eqs. (2.9).

Let the density perturbation $\rho(\eta, \xi, \tau)$ and the potential perturbation $\Psi(\eta, \xi, \tau)$ be expressed by

$$\rho(\eta, \xi, \tau) = \sum_{n=1}^{\infty} \sum_{m=-\infty}^{\infty} \bar{\rho}_{nm}(\tau) \sin(n\pi\eta) \exp(im\pi\xi)$$

$$\Psi(\eta, \xi, \tau) = \sum_{n=1}^{\infty} \sum_{m=-\infty}^{\infty} \bar{\Psi}_{nm}(\tau) \sin(n\pi\eta) \exp(im\pi\xi) \qquad (3.6)$$

Here the choice of the sine series in the x direction satisfies the boundary conditions, and we use a discrete wave spectrum with a fundamental wave number of $\pi/(\Lambda d)$ to approximate the continuous wave spectrum in the z direction. We substitute the Fourier series in (3.6) into Eqs. (3.3) and (3.4) and obtain the following system of equations

$$\frac{\partial \bar{\rho}_{nm}}{\partial \tau} = -A_1\pi^2\left[n^2 + \left(\frac{m}{\Lambda}\right)^2 \right]\bar{\rho}_{nm} - iA_2\pi\frac{m}{\Lambda}\bar{\rho}_{nm}$$

$$- A_1\pi^2\left[n^2 + \left(\frac{m}{\Lambda}\right)^2 \right]\bar{\Psi}_{nm} + i2\pi\frac{m}{\Lambda}\bar{\Psi}_{nm} \qquad (3.7)$$

$$- \pi A_3\left[n U_{nm} + \frac{m}{\Lambda} V_{nm} \right] + i\pi^2 W_{nm}$$

$(n = 1, 2, 3, \text{----}, m = 0, \pm 1, \pm 2, \text{----})$

$$B_1\pi^2\left[n^2+\left(\frac{m}{\Lambda}\right)^2\right]\bar{\rho}_{nm} + iB_2\pi\frac{m}{\Lambda}\bar{\rho}_{nm}$$
$$+ B_3\pi^2\left[n^2+\left(\frac{m}{\Lambda}\right)^2\right]\bar{\psi}_{nm} \qquad (3.8)$$
$$+ 2\pi B_4\left[nU_{nm}+\frac{m}{\Lambda}V_{nm}\right] = 0$$

$(n = 1, 2, 3 \text{ ----}, m = 0, \pm 1, \pm 2, \text{ ----})$

where U_{nm}, V_{nm} and W_{nm} are terms bilinear in $\bar{\rho}_{ij}$ and $\bar{\psi}_{ij}$ and represent interactions between various modes.

$$U_{nm} = \sum_{\ell=1}^{\infty}\sum_{q=-\infty}^{\infty}\ell\bar{\psi}_{\ell q}\left\{\sum_{j=1,2}^{\infty}\bar{\rho}_{j(m-q)}\left[\frac{j}{j^2-(\ell-n)^2}+\frac{j}{j^2-(\ell+n)^2}\right]\right\}$$

$$V_{nm} = \sum_{\ell=1}^{\infty}\sum_{q=-\infty}^{\infty}\frac{q}{\Lambda}\bar{\psi}_{\ell q}\left\{\sum_{j=1,2}^{\infty}\bar{\rho}_{j(m-q)}\left[\frac{j}{j^2-(\ell-n)^2}-\frac{j}{j^2-(\ell+n)^2}\right]\right\}$$

Here the summation on j is over odd integers if $\ell \pm n$ is even or zero and is over even integers if $\ell \pm n$ is odd.

$$W_{nm} = \sum_{\ell=1}^{\infty}\sum_{q=-\infty}^{\infty}\frac{1}{\Lambda}\left[(\ell m+nq)\bar{\psi}_{\ell q}\,\bar{\rho}_{(n+\ell)(m-q)} + (\ell m-nq)\,\mathrm{sgn}(n-\ell)\bar{\psi}_{\ell q}\,\bar{\rho}_{|n-\ell|(m-q)}\right]$$

Here $\mathrm{sgn}(n) = n/|n|$ if $n \neq 0$ and $\mathrm{sgn}(0) = 0$.

Computations restrict us to a finite sub-system of these equations. We use the finite sum

$$\rho(\eta,\xi,\tau) = \sum_{n=1}^{N}\sum_{m=-M}^{M}\bar{\rho}_{nm}(\tau)\,\sin(n\pi\eta)\,\exp(im\pi\xi) \qquad (3.9)$$

$$\psi(\eta,\xi,\tau) = \sum_{n=1}^{N}\sum_{m=-M}^{M}\bar{\psi}_{nm}(\tau)\,\sin(n\pi\eta)\,\exp(im\pi\xi)$$

to approximate the series in (3.6) and restrict n and m in Eqs. (3.7) and (3.8) to $1 \le n \le N$ and $0 \le |m| \le M$. The series in the expressions for U_{nm}, V_{nm} and W_{nm} are simply terminated by choosing $\bar{\rho}_{ij} = \bar{\Psi}_{ij} = 0$ whenever $i > N$ or $|j| > M$. We also make use of the reality conditions, $\bar{\rho}^*_{nm} = \bar{\rho}_{n(-m)}$ and $\bar{\Psi}^*_{nm} = \bar{\Psi}_{n(-m)}$ where the asterisk indicates the complex conjugate. Thus we can further restrict the index m to $0 \le m \le M$ and obtain $2 \times N \times (2M + 1)$ real equations from Eqs. (3.7) and (3.8) for $2 \times N \times (2M + 1)$ real unknowns, namely, $(\bar{\rho}_{no}, \bar{\rho}^R_{nm}, \bar{\rho}^I_{nm})$ and $(\bar{\Psi}_{no}, \bar{\Psi}^R_{nm}, \bar{\Psi}^I_{nm})$ where $1 \le n \le N$, $1 \le m \le M$ and the superscripts R and I denote the real and imaginary parts respectively.

In carrying out the time integration, we used Hamming's modified predictor-corrector method with a special Runge-Kutta procedure for starting values. It is a stable fourth-order integration procedure. The routine for evaluating the time derivative $\partial \bar{\rho}_{nm}/\partial\tau$ is as follows. First, the spectral density $\bar{\rho}_{nm}$ for all n and m are given as initial values or obtained from the previous time step. We then solve the system of linear algebraic Eqs. (3.8) in the unknown potentials $\bar{\Psi}_{nm}$. Second, $\partial \bar{\rho}_{nm}/\partial\tau$ is then evaluated using Eq. (3.7).

It is essential that the solutions of Eqs. (3.8) be sufficiently accurate in each step that rounding errors can never accumulate to any great extent. We used a Gaussian reduction method with iterative refinements.[5] The diagonal dominant property of the coefficient matrix enables us to obtain solutions with 6 digit accuracy in the norm of the solution vector in a few iterations. The time step used in integration must also be smaller than the period of the fastest motion of the system. We chose the time step such that the estimate of the local truncation error given by the predictor-corrector method is always less than 10^{-6}. It is also necessary that N and M be chosen sufficiently large that enough modes be included in the calculations. We

have no mathematical criterion for the requirement on N and M. However, one can see from Fig. 2 that modes with $n > 2$ are heavily damped when the instability first sets in for modes of $n = 1$. We therefore chose $N = 2$ and neglected any modes with $n > 2$. In addition, one can see that, for $H > H_c$, only modes with an axial wavenumber k in the band $k_1 < k < k_2$ have positive growth rates. We chose our modes centered around these modes. Choosing $M = \Lambda^2$ with $\Lambda = 2, 3, 4$ successively, we increased the number of modes included as well as the fundamental wavelength. A finite number of modes might be sufficient to describe the system if modes at both ends of the spectrum remain at low level during the time of interest.

The following numerical values of system parameters are used in computation. $b^-/b^+ = 10^2$, $T^-/T^+ = 20$, $\delta s/s = 10^{-3}$ and $d/R = 10^{-5}$. Notice that the inequality (2.6) is satisfied.

4. Results in the Slightly Super-Critical Regime

We first investigated the evolution of an initial white-noise-like disturbance when the magnetic field is slightly above the critical value H_c. We assumed as initial values $|\rho_{nm}| = 10^{-3}$ for all n and m with the initial phase determined by random numbers.

Fig. 3 shows the time development of various modes at $H = 1.05\ H_c$ under the assumption of $N = 2$, $\Lambda = 2$ and $M = 4$. The numbers of each curve represent the mode number n and m defined in Eq. (3.9). Initially the various modes are observed to grow or decay exponentially in time. This is what one expects since the initial perturbations are small and linear analysis giving exponential growth or decay should be valid. The initial growth rate and

oscillating frequency of each mode are in good agreement with that given by Eq. (2.10) of the linear analysis. Thus we have a good check on our computing codes. One notices in Fig. 3 the growth of the mode with n = 2, m = 0 as well as the critical mode n = 1, m = 2. The mode (2, 0) represents a modification to the equilibrium density. Its sign (not shown in the figure) is negative so as to reduce the equilibrium density in the region near the inner cylinder and increase it near the outer wall. That is, it acts to flatten the density gradient which is what we expect the nonlinear correction to do. Due to this change in equilibrium density, the critical mode (1, 2) levels off subsequently and a final steadily oscillating state with the saturation amplitude shown is reached. The final oscillating frequency is also shifted from that given by linear analysis evaluated at the critical field.

We ran another computation under the same conditions, however, with the number of modes increased by choosing N = 2, Λ = 3, M = 9. The results are shown in Fig. 4. The same final oscillating state as in the previous case is reached with the critical mode labeled (1,3) because of the different value of Λ assumed.

Fig. 5 shows the results obtained at H = 1.1 H_c. Notice that three modes (1, 2), (1, 3), and (1, 4) are located in the unstable wave band and they all have initial positive growth rates. Some of the modes like (1, 5), (1, 1), and (2, 1) which decay initially are excited through mode interactions. However all modes finally subside except the oscillating critical mode (1, 3) with an axial wavenumber k = π/d and the time independent modification given by the mode (2, 0).

We also ran computations at other field values. To summarize our computed results in the slightly super-critical regime, we plot as functions of magnetic field the difference $\delta\omega$ between the final oscillation frequency and the linear oscillation frequency evaluated at the critical field (Fig. 6), the squared final oscillation amplitude of the density wave and the magnitude of the time independent change in the equilibrium density (Fig. 7), and the squared final oscillation amplitude of the potential wave and the magnitude of the time independent change in the equilibrium potential (Fig. 8). In these figures, we also plot the analytic results obtained from Eqs (3.10), (3.11), (4.7), (4.8), and (2.23) of I. The analytic results are valid in the limit $\Delta = (H-H_c)/H_c \ll 1$. It is seen indeed that the analytic results and our numerical results are in good agreement in this limit.

5. Results at Higher Magnetic Fields

We tried next to extend our computation with the magnetic field increased further. To include more modes in the unstable wave band $k_1 < k < k_2$, we chose $\Lambda = 4$ and $M = 16$. Fig. 9 shows the time development of various modes at $H = 1.3\ H_c$. Only modes with amplitude larger than 10^{-4} at $\tau = 30$ are shown in the figure. It is seen that initially each mode grows or decays much more rapidly because of the increased magnetic field. Some of the modes which decay initially begin to grow in a short time. These include the mode (2, 1) and some other modes not shown in the figure. After a period of interactions, all these modes as well as those which grow initially begin to subside leaving a steady oscillation of the mode (1, 3) with an axial wavenumber $k = 1.25\ \pi/d$, and the mode (2, 0) giving the time independent change of the equilibrium distribution. Fig. 10 shows a similar evolution

of modes at $H = 1.6\ H_c$. In this case, however, the final oscillation is dominated by mode (1, 6) which has an axial wavenumber $k = 1.5\ \pi/d$. The modes (1, 5) and (1, 6) happen to be the modes with the largest growth rates at $H = 1.3\ H_c$ and $H = 1.6\ H_c$ respectively. Their rapid growth seems to enable them to take over the other modes.

To study more closely the problem of wavenumber selection, we ran some computations under the assumption of a weighted initial disturbance. That is, we put the initial magnitude of one of the modes in the unstable wave band $k_1 < k < k_2$ at larger magnitude than the rest. To be more specific, we put the weighted amplitude at 2×10^{-3} and the other amplitudes at 10^{-4}. Fig. 11 shows results obtained at $H = 1.3\ H_c$ with the assumption of such a weighted initial amplitude for the mode (1, 6). It is seen that stable final oscillation with the dominance of the mode (1, 6), instead of the mode (1, 5), can be established. The weighted initial amplitude of the mode (1, 6) is sufficiently strong that it can dominate and force down other modes which have larger initial growth rates. Fig. 12 shows the results obtained at $H = 1.3\ H_c$ with the mode (1, 7) weighted. Contrary to the previous case, final oscillation with the mode (1, 7) cannot be reached. The mode (1, 7) seems unstable with respect to perturbation of other modes and the mode (1, 5), which has the largest linear growth rate, takes over and finally dominates. Out of the seven modes (m = 2, 3, ---8) inside the unstable wave band at $H = 1.3\ H_c$, we find it possible to establish final stable oscillations of the mode with m = 4, 5, or 6 if the particular mode has its initial amplitude weighted with respect to the rest as described. Similarly, we find that, at $H = 1.6\ H_c$, it is possible to establish stable final oscillation of the mode with m = 4, 5, 6, 7, or 8 out of the ten modes (m = 2, 3, ---11) inside the unstable wave band.

6. Discussion

We would like to point out that the final state of the plasma indicated by our computed results is in sharp contrast with that obtained by Sato and Tsuda[2] for the case of the cross-field instability. Their computed results indicate that the instability develops explosively into a strong turbulence, while we have the dominance of a single finite amplitude mode up to $H = 1.6\ H_c$. We do not have direct experimental support for the dominance of the single mode. However recent experimental work[6] on a similar macroscopic instability in a weakly ionized plasma, namely the spiral instability of the positive column, indicates the dominance of a single mode for magnetic field strengths up to many times the critical value. Transition from laminar convection to turbulent convection could possibly occur at higher magnetic fields than those we investigated here. We do not go to higher magnetic fields because of the increased number of modes needed and the increased computing time.

We would also like to mention that the idea of studying the wavenumber selection problem using a computational approach has been mentioned in the work of DiPrima and Rogers.[7] The nonuniqueness of the wavelength of the supercritical flow also occurs in some nonlinear hydrodynamic instabilities. The experimental work of Snyder[8] indicates the possibility of obtaining Taylor-vortex flows of different wavelengths.

In summary, our numerical investigation shows that a weakly ionized plasma in a strong and nonuniform magnetic field is subject to an instability. Upon the onset of the instability, convective flow develops in the plasma and a final steadily oscillating state, dominated by a single finite amplitude mode together with a time independent modification of the original equilibrium, is reached. The final oscillating state approaches that given by the analytic results of Simon[4] in the limit $H \to H_c$. We find the dominance of a

single mode up to $H = 1.6\ H_c$. However, the wavelength of the final oscillation reached is nonunique and depends on initial conditions. For initial white-noise-like disturbances, we find that the mode with the largest linear growth rate will force down other modes and dominate. For weighted initial disturbances, we find there exists a subinterval of wavenumbers inside the unstable wave band. Final stable oscillation with a certain wavelength in this subinterval can be established, if the initial disturbance has a sufficiently strong component at the particular wavelength.

ACKNOWLEDGMENTS

The author wishes to express his sincere thanks to Dr. T. J. Birmingham for his continual interest and helpful suggestions in improving the text.

References

1. A. Simon, Phys. Fluids 11, 1181 (1968).
2. T. Sato and T. Tsuda, Phys. Fluids 10, 1262 (1967).
3. B. B. Kadomtsev, Plasma Turbulence (Academic Press Inc., New York, 1965), p. 7.
4. A. Simon, Phys. Fluids 11, 1186 (1968).
5. G. E. Forsythe and C. B. Moler, Computer Solution of Linear Algebraic Systems (Prentice Hall Inc., Englewood Cliffs, N. J., 1967).
6. M. W. Halseth and R. V. Pyle, Phys. Fluids 13, 1238 (1970).
7. R. C. DiPrima and E. H. Rogers, Phys. Fluids Suppl. II, 12, II-155, (1969).
8. H. A. Snyder, J. Fluid Mech. 35, 273 (1969).

Figure Captions

Figure 1. Geometry of the problem and picture of instability mechanism. Darkened areas indicate density enhancement due to perturbation. + and - signs indicate polarization charges resulting from oppositely directed drifts of electrons and ions.

Figure 2. Neutral stability curve of magnetic field H versus axial wavenumber k for various radial wavenumbers n. The plasma is stable for $H < H_c$. The dashed line represents a band of unstable wavenumber at the operating magnetic field.

Figure 3. Evolution of Fourier components of density wave at $H = 1.05\ H_c$ for the case of white-noise-like initial disturbance. The curves are labeled according to the mode numbers n and m. Those modes not shown in the figure decay to less than 10^{-4} before $\tau = 1$.

Figure 4. Evolution of Fourier components of density wave at $H = 1.05\ H_c$ for the case of white-noise-like initial disturbance. The curves are labeled according to the mode numbers n and m. Those modes not shown in the figure decay to less than 10^{-4} before $\tau = 2$.

Figure 5. Evolution of Fourier components of density wave at $H = 1.1\ H_c$ for the case of white-noise-like initial disturbance. The curves are labeled according to the mode numbers n and m. Those modes not shown in the figure decay to less than 10^{-4} before $\tau = 3$.

Figure 6. Comparison of the frequency shift $\delta\omega$ as a function of magnetic field H from analytic results (line) and that from present numerical results (circles). $\delta\omega$ is the difference between the final oscillation frequency and the linear oscillation frequency evaluated at the critical field ω_c^R.

Figure 7. Comparison of the squared final amplitude of the density wave $|\rho_{1\Lambda}|^2$ and the magnitude of the time independent modification to the equilibrium density $|\rho_{20}|$ as functions of magnetic field H obtained from analytic results (lines) and from present numerical results (squares and circles).

Figure 8. Comparison of the squared final amplitude of the potential wave $|\Psi_{1\Lambda}|^2$ and the magnitude of the time independent modification to the equilibrium potential $|\Psi_{20}|$ as functions of magnetic field H obtained from analytic results (lines) and from present numerical results (squares and circles).

Figure 9. Evolution of Fourier components of density wave at $H = 1.3\ H_c$ for the case of white-noise-like disturbance. The curves are labeled according to the mode numbers n and m. Those modes not shown in the figure have magnitude less than 10^{-4} for $\tau \geq 30$.

Figure 10. Evolution of Fourier components of density wave at $H = 1.6\ H_c$ for the case of white-noise-like disturbance. The curves are labeled according to the mode numbers n and m. Those modes not shown in the figure have magnitude less than 10^{-4} for $\tau \geq 40$.

Figure 11. Evolution of Fourier components of density wave at $H = 1.3\ H_c$ for the case of weighted initial disturbance. The curves are labeled according to the mode numbers n and m. The mode with n = 1 and m = 6 is the weighted component. Only the mode (2, 0) and modes with initial positive growth rate are shown in the figure.

Figure 12. Evolution of Fourier components of density wave at $H = 1.3\ H_c$ for the case of weighted initial disturbance. The curves are labeled according to the mode numbers n and m. The mode with n = 1 and m = 7 is the weighted component. Only the mode (2, 0) and modes with initial positive growth rate are shown in the figure.

R
H
HΔ
NΔ
E2

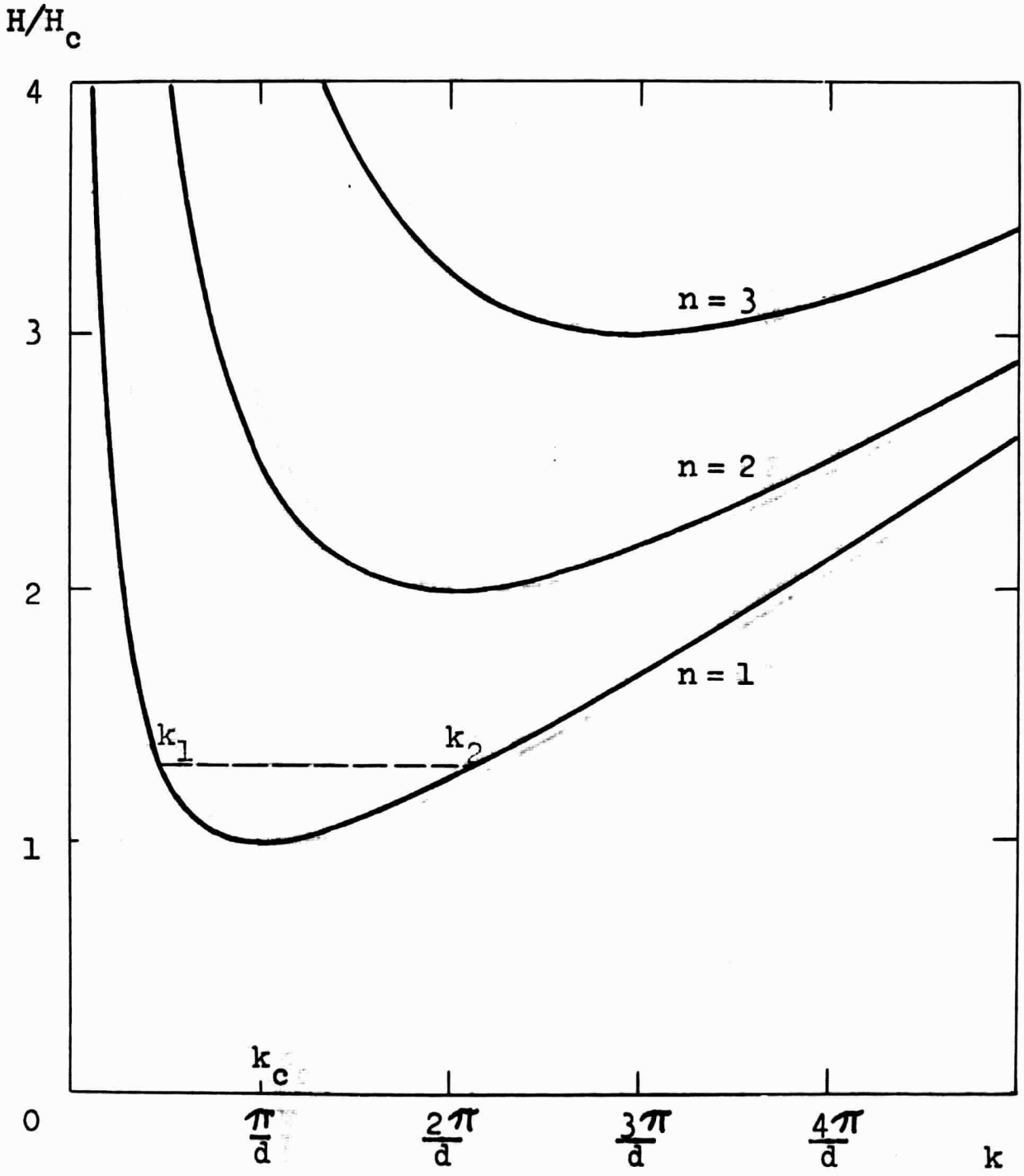
H/H_c
4
3
2
1
0
n = 3
n = 2
n = 1
k_1
k_2
k_c
π/d
2π/d
3π/d
4π/d
k

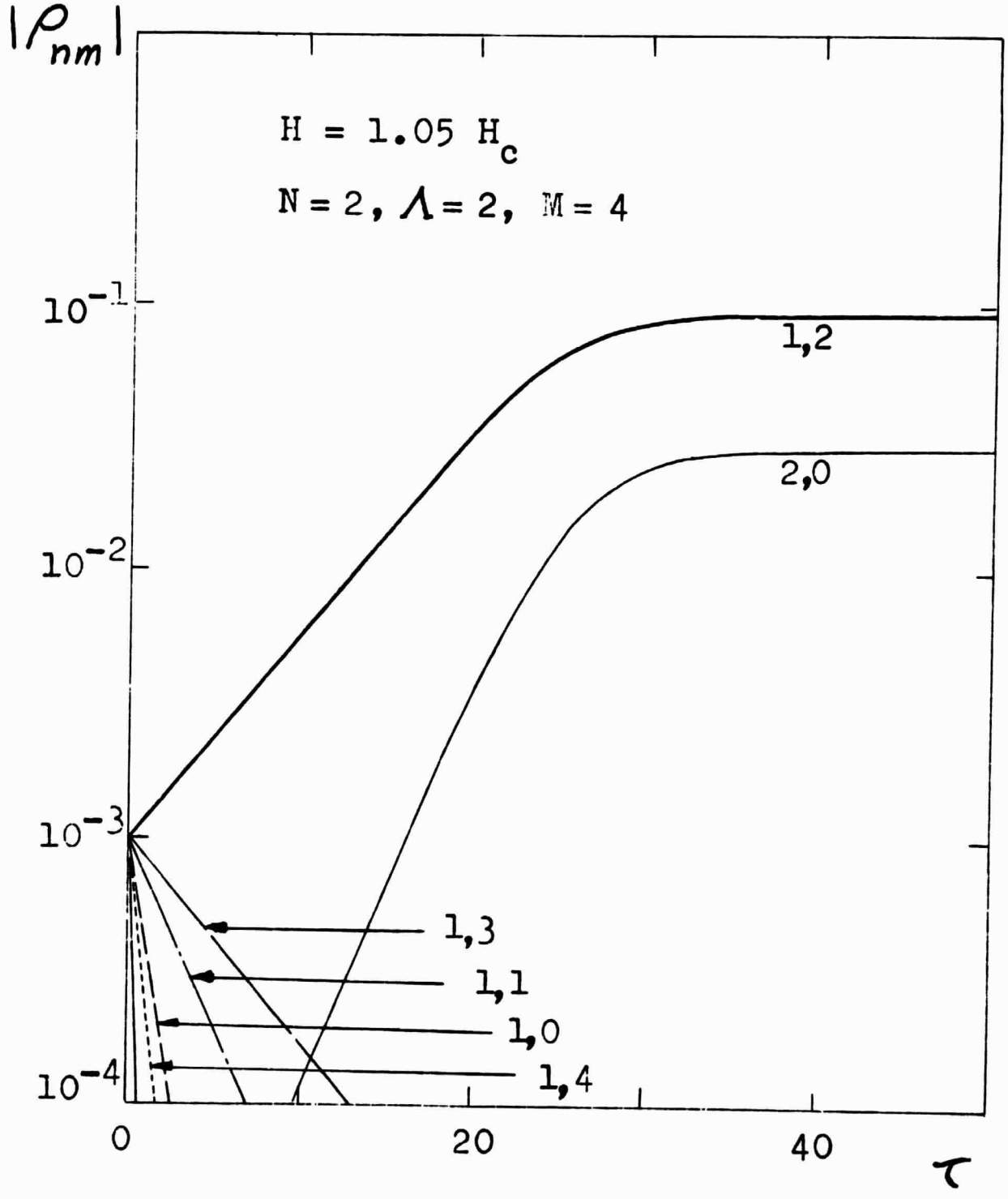
$|\rho_{nm}|$
H = 1.05 H_c
N = 2, Λ = 2, M = 4
10^{-1}
10^{-2}
10^{-3}
10^{-4}
1,2
2,0
1,3
1,1
1,0
1,4
0
20
40
τ

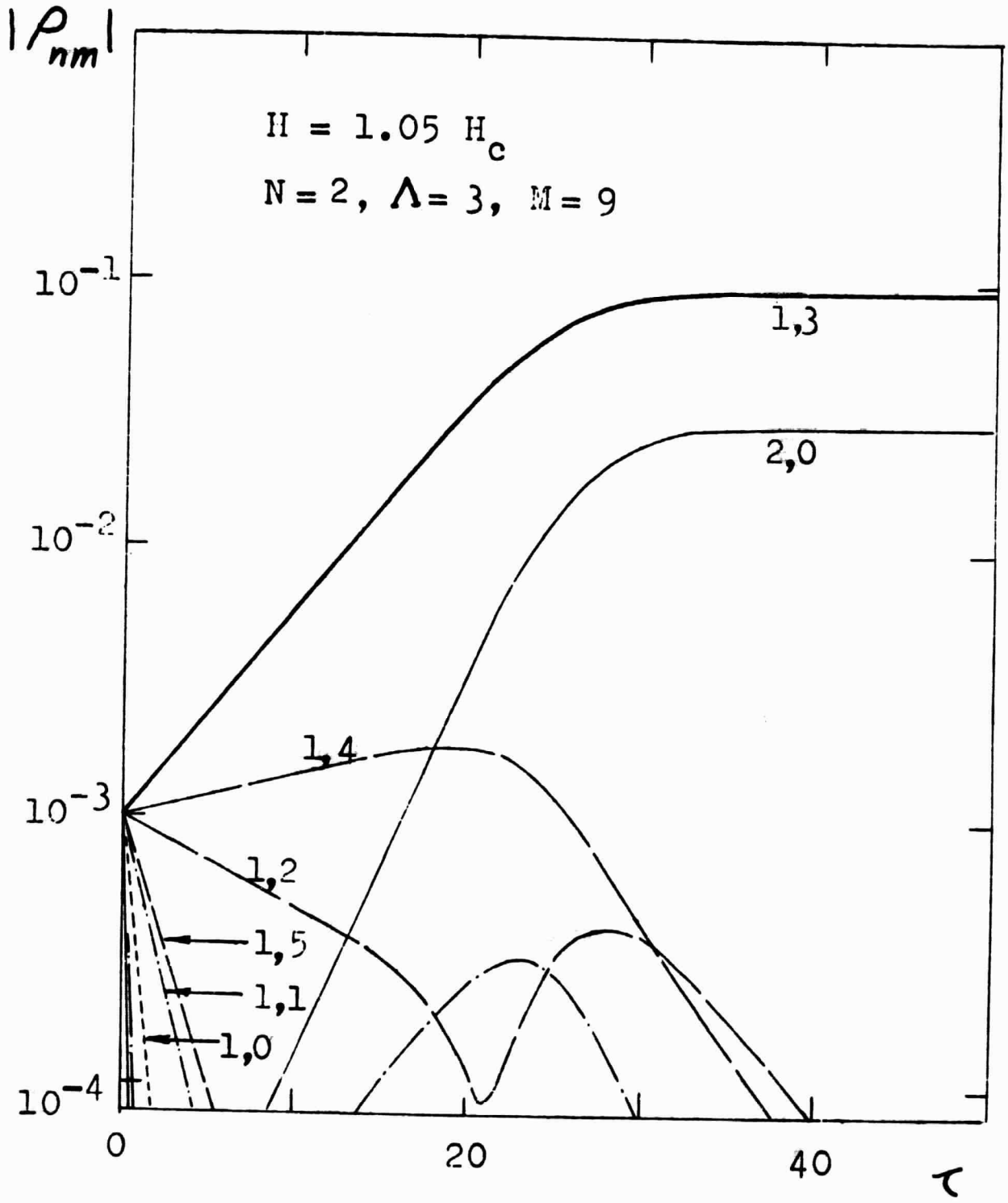
$|\rho_{nm}|$
H = 1.05 H_c
N = 2, Λ = 3, M = 9
10^{-1}
10^{-2}
10^{-3}
10^{-4}
1,3
2,0
1,4
1,2
1,5
1,1
1,0
0
20
40
τ

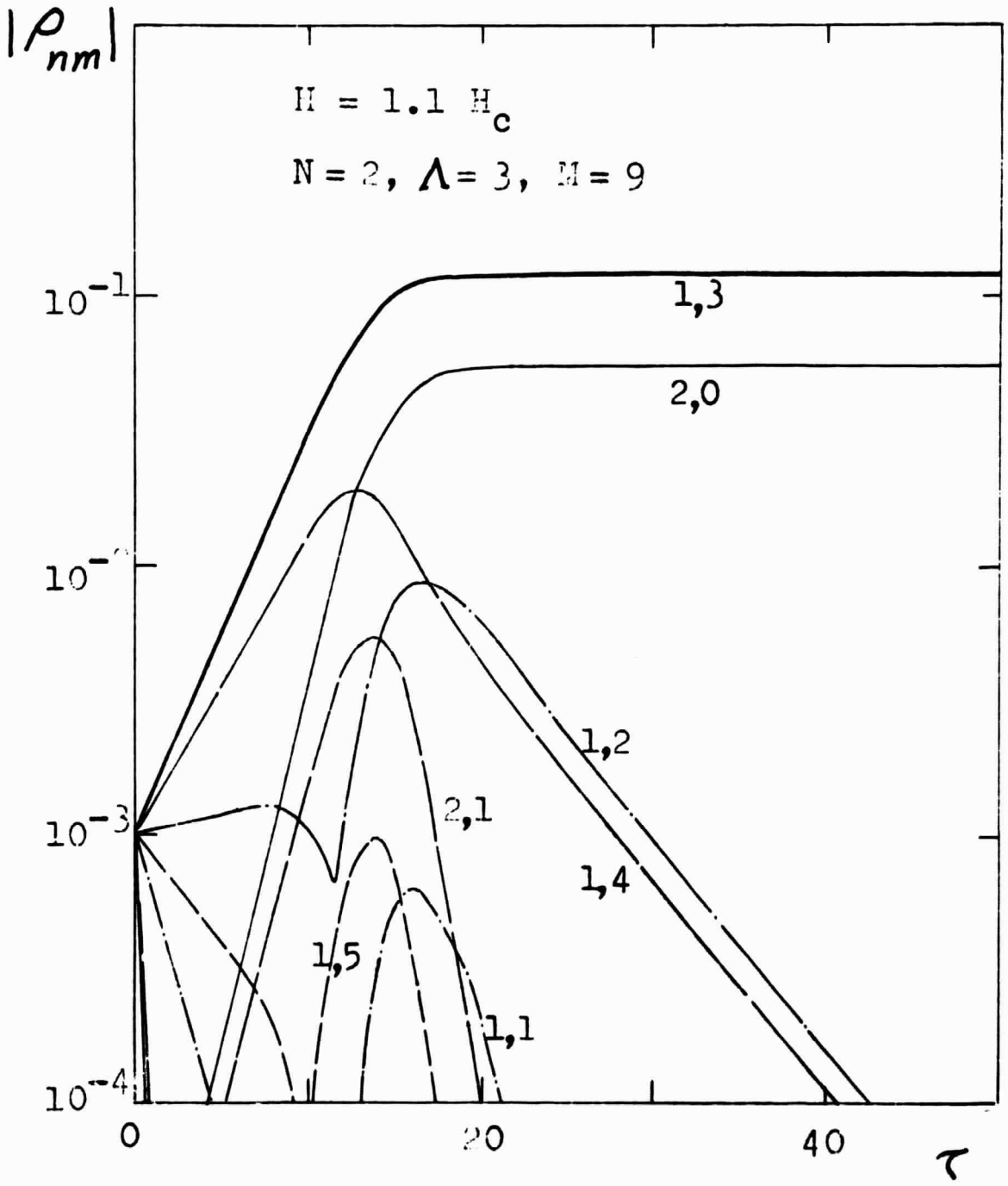
$|\rho_{nm}|$
H = 1.1 H_c
N = 2, Λ = 3, M = 9
10^{-1}
10^{-2}
10^{-3}
10^{-4}
1,3
2,0
1,2
2,1
1,4
1,5
1,1
0
20
40
τ

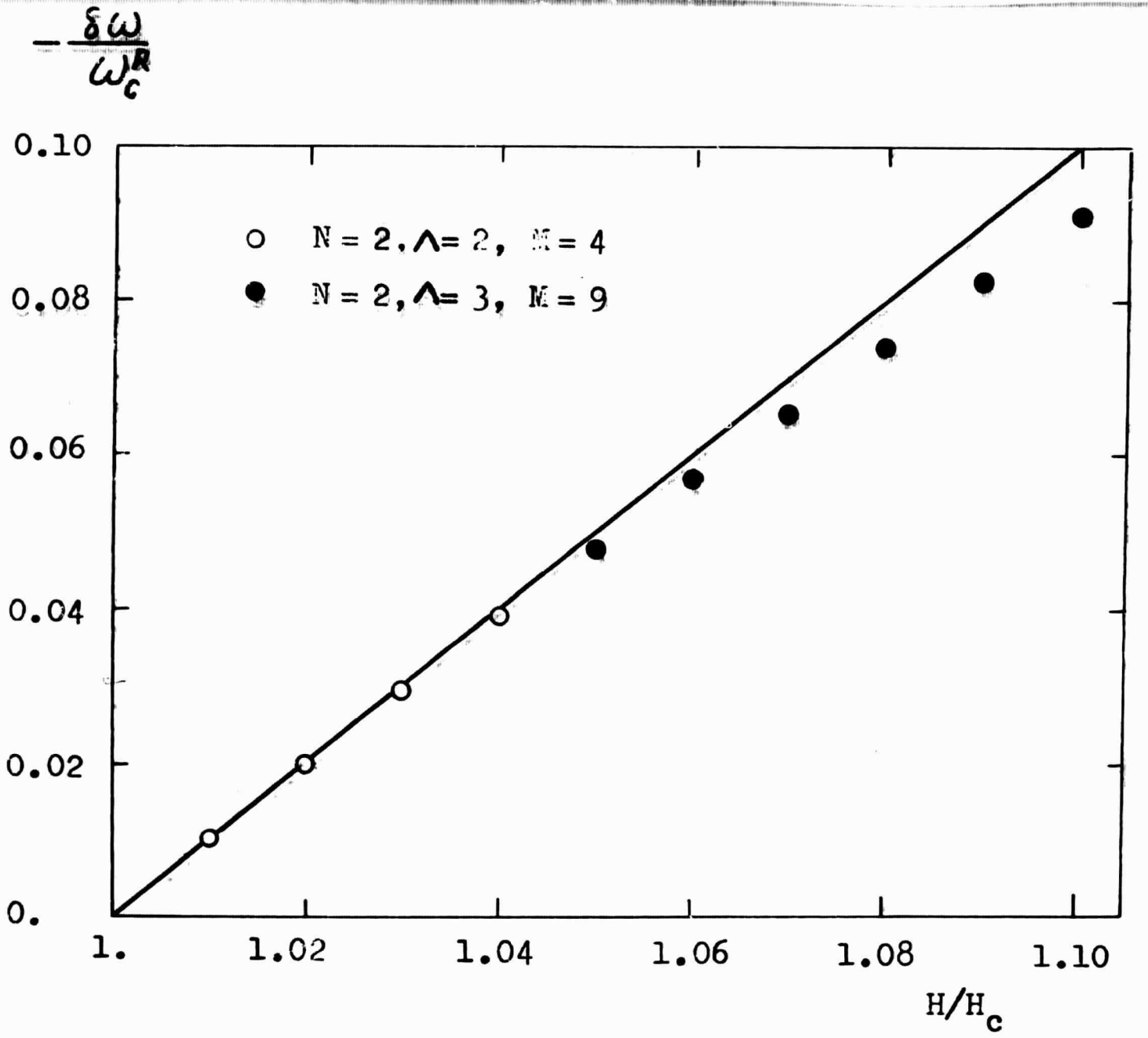
$-\frac{\delta\omega}{\omega_c^R}$
0.10
0.08
0.06
0.04
0.02
0.
1.
1.02
1.04
1.06
1.08
1.10
H/H_c
N = 2, Λ= 2, M = 4
N = 2, Λ= 3, M = 9

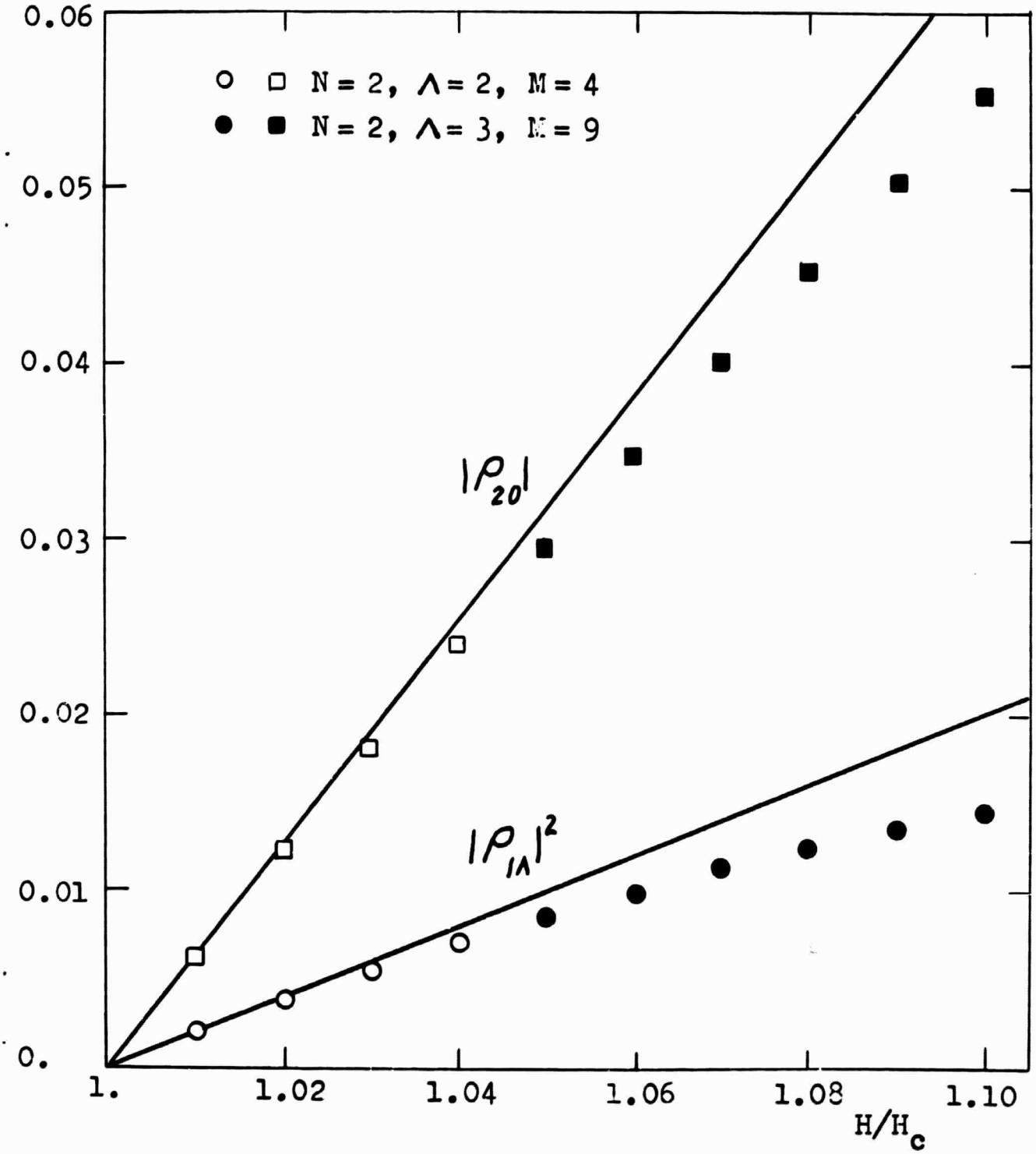
0.06
0.05
0.04
0.03
0.02
0.01
0.
N = 2, Λ = 2, M = 4
N = 2, Λ = 3, M = 9
$|\rho_{20}|$
$|\rho_{1\Lambda}|^2$
1.
1.02
1.04
1.06
1.08
1.10
H/H_c

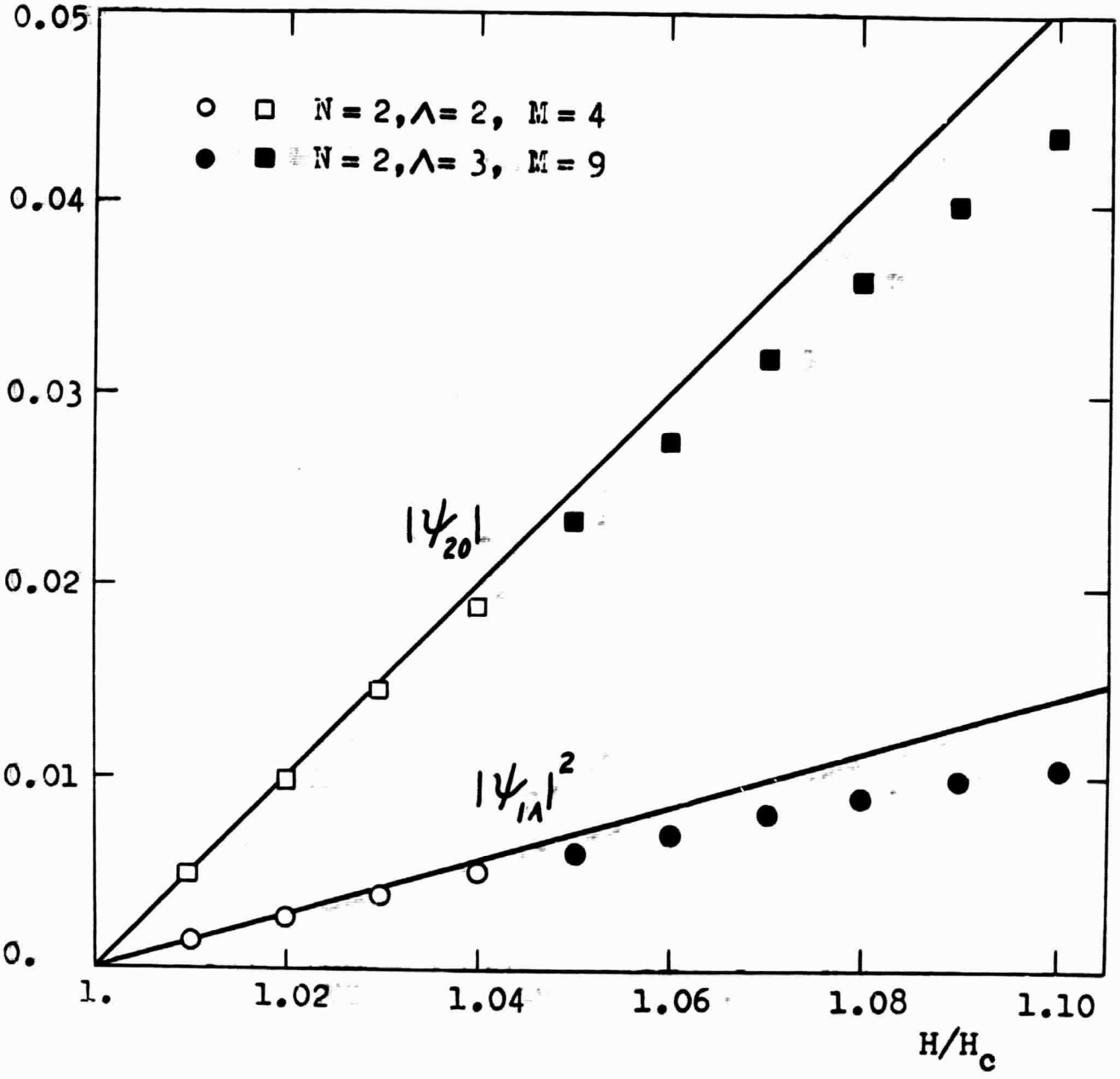
0.05
0.04
0.03
0.02
0.01
0.
N = 2, Λ = 2, M = 4
N = 2, Λ = 3, M = 9
$|\psi_{20}|$
$|\psi_{11}|^2$
1.
1.02
1.04
1.06
1.08
1.10
H/H_c

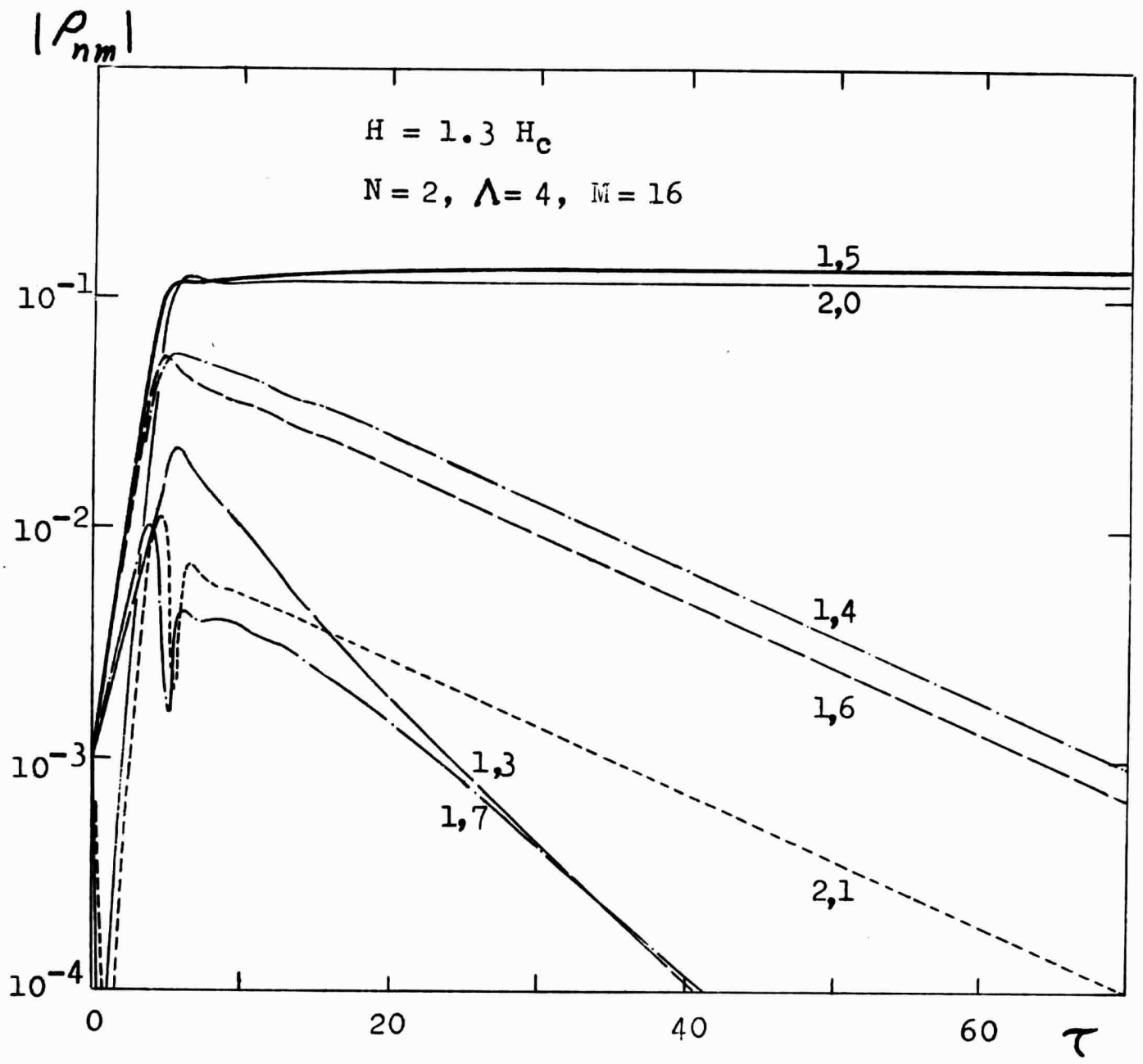
$|\rho_{nm}|$
H = 1.3 H_c
N = 2, Λ = 4, M = 16
1,5
2,0
1,4
1,6
1,3
1,7
2,1
10^{-1}
10^{-2}
10^{-3}
10^{-4}
0
20
40
60
τ

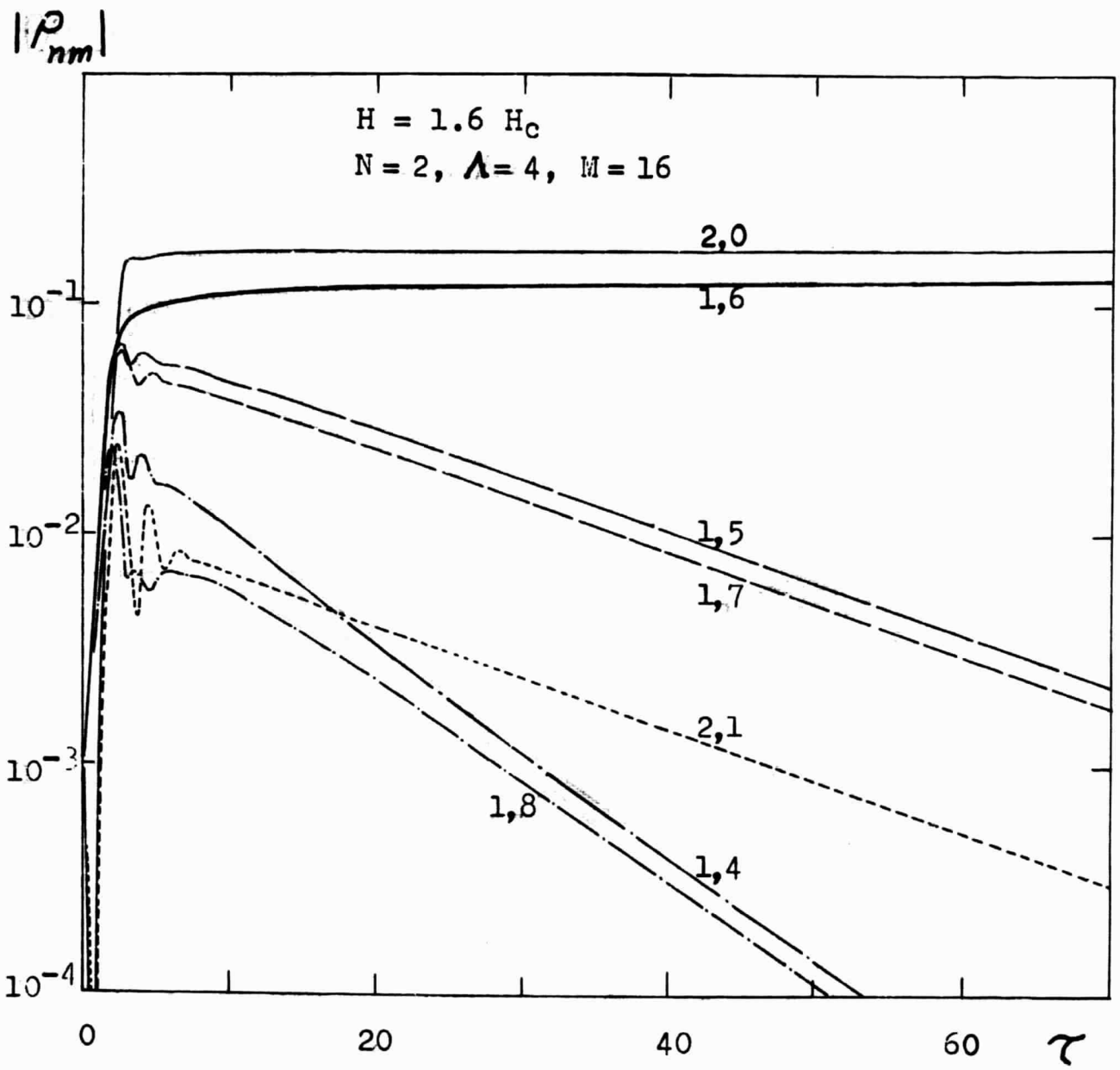
$|\rho_{nm}|$
H = 1.6 H_c
N = 2, Λ = 4, M = 16
2,0
1,6
1,5
1,7
2,1
1,8
1,4
10^{-1}
10^{-2}
10^{-3}
10^{-4}
0
20
40
60
τ

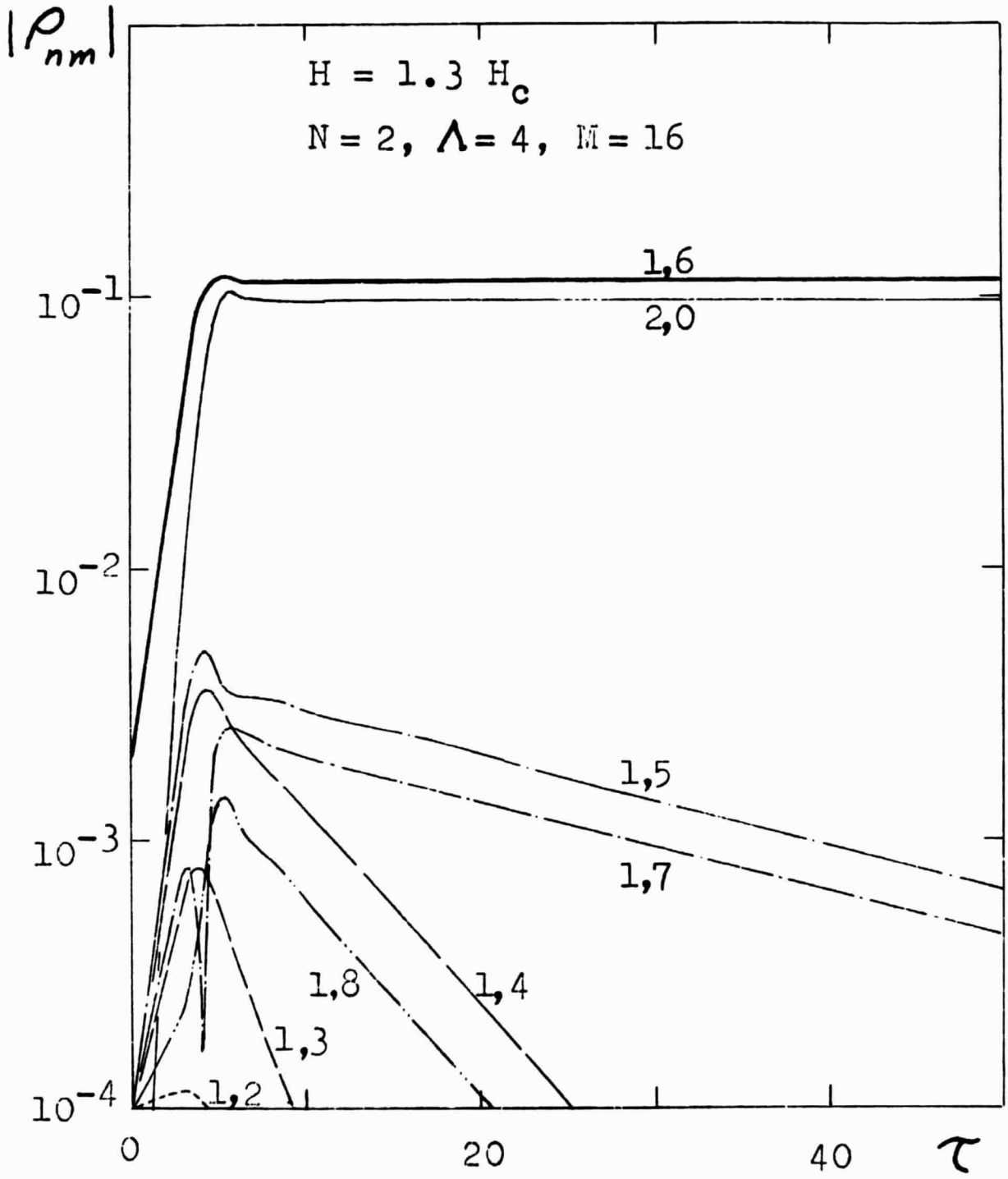
$|\rho_{nm}|$
H = 1.3 H_c
N = 2, Λ = 4, M = 16
1,6
2,0
1,5
1,7
1,8
1,4
1,3
1,2
10^{-1}
10^{-2}
10^{-3}
10^{-4}
0
20
40
τ

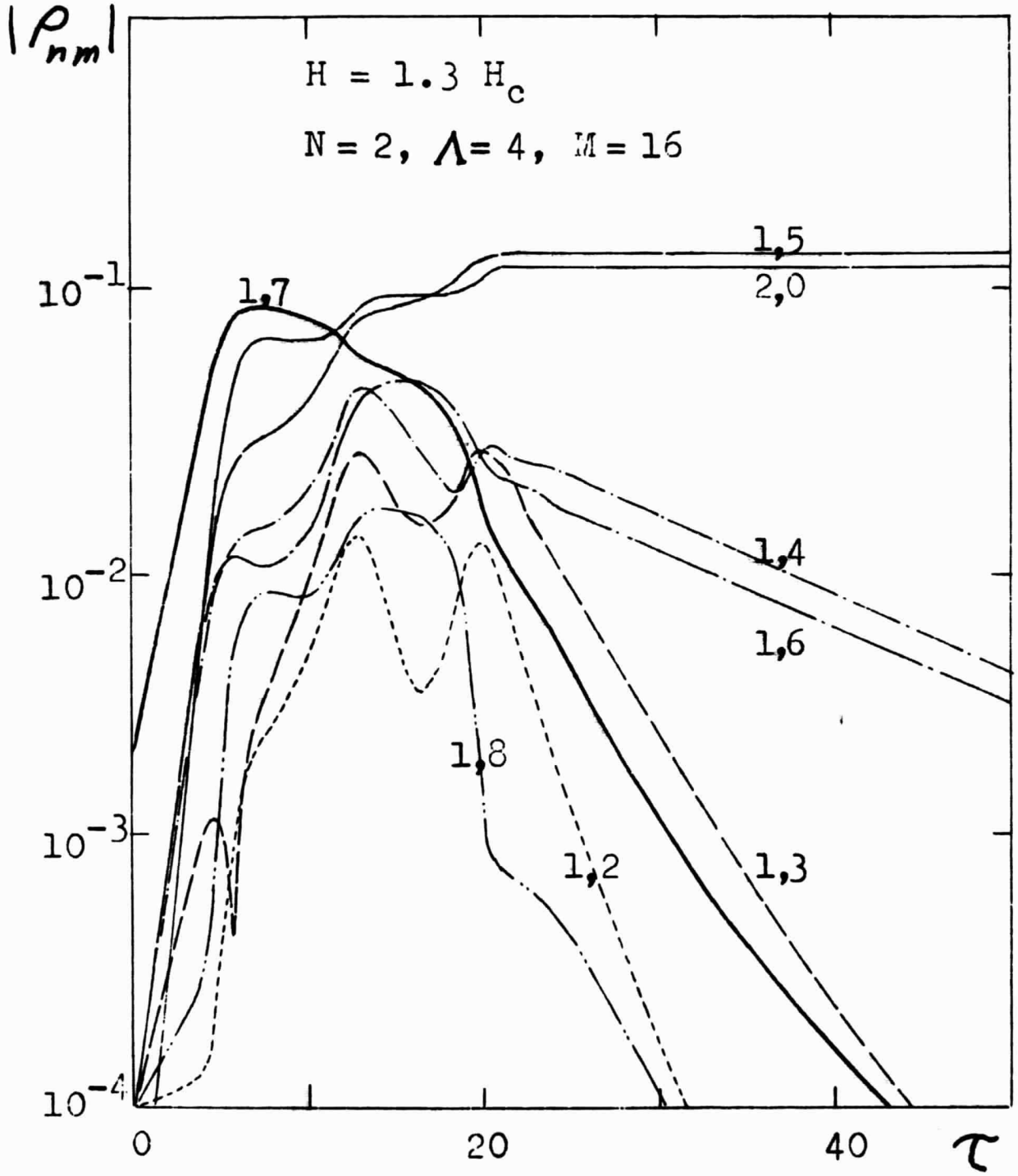
$|\rho_{nm}|$
H = 1.3 H_c
N = 2, Λ = 4, M = 16
1,5
2,0
1,7
1,4
1,6
1,8
1,2
1,3
10^{-1}
10^{-2}
10^{-3}
10^{-4}
0
20
40
τ